European Polymer Journal 159 (2021) 110754

Contents lists available at ScienceDirect

European Polymer Journal

journal homepage: www.elsevier.com/locate/europolj

N-butylamine-modified graphite nanoflakes blended in ferroelectric P(VDF-TrFE) copolymers for piezoelectric nanogenerators with high power generation efficiency

Tzu-Chuan Yang [a], Yi-Pei Jiang [a], Ting-Han Lin [b], Shih-Hsuan Chen [b], Ching-Mei Ho [b], Ming-Chung Wu [b,c,d], Jer-Chyi Wang [a,c,e,f,*]

[a] Department of Electronic Engineering, Chang Gung University, Guishan Dist. 33302, Taoyuan, Taiwan
[b] Department of Chemical and Materials Engineering, Chang Gung University, Guishan Dist. 33302, Taoyuan, Taiwan
[c] Green Technology Research Center, Chang Gung University, Guishan Dist. 33302, Taoyuan, Taiwan
[d] Division of Neonatology, Department of Pediatrics, Chang Gung Memorial Hospital, Linkou, Guishan Dist. 33305, Taoyuan, Taiwan
[e] Department of Neurosurgery, Chang Gung Memorial Hospital, Linkou, Guishan Dist. 33305, Taoyuan, Taiwan
[f] Department of Electronic Engineering, Ming Chi University of Technology, Taishan Dist. 243303, New Taipei City, Taiwan

ARTICLE INFO

Keywords:
Graphite
Nanoflake
Poly(vinylidenefluoride-co-trifluoroethylene) (P(VDF-TrFE))
Piezoelectric
Nanogenerator

ABSTRACT

In this study, the effects of n-butylamine-modified graphite nanoflakes (BMGNFs) on the crystalline phase transition, ferroelectric behaviors, and piezoelectric energy harvesting properties of poly(vinylidenefluoride-co-trifluoroethylene) (P(VDF-TrFE)) copolymers are investigated. To confirm the blending of BMGNFs in P(VDF-TrFE), X-ray spectroscopy and Fourier-transform infrared spectroscopy (FTIR) are performed. Additionally, X-ray diffraction, FTIR, field-emission scanning electron microscopy, and atomic force microscopy are performed to analyze the crystallization of the polar β-phase of BMGNF-blended P(VDF-TrFE) copolymers. For P(VDF-TrFE) copolymers blended with pure graphite nanoflakes (GNFs), the crystallization of the polar β-phase is enhanced, but a high dielectric loss induced by the leakage current is clearly observed. The dielectric loss can be effectively reduced through the modification of GNFs by n-butylamine, which improves the remnant polarization and coercive electric field of metal-ferroelectric-semiconductor devices. Furthermore, the piezoelectric nanogenerators comprising BMGNF-blended P(VDF-TrFE) copolymers present a high open-circuit output voltage of 4.9 V and a high short-circuit output current of 4.5 μA for more than 500 times of cycling tests, exhibiting a high generating power density of 33.73 mW/m^2 under a load resistance of 3 MΩ. Hence, the P(VDF-TrFE) copolymers blended with n-butylamine-modified GNFs show superior ferroelectric and piezoelectric behaviors, rendering them promising candidates for applications in future organic sensors and self-powered consumer electronics.

1. Introduction

Electricity shortage has become a severe issue that hinders the development of the industry and economy. Fossil fuel depletion, also known as energy crisis, will occur in the mid-21st century because approximately 64 % of the global electricity originated from fossil fuels [1]. According to Solomon's prediction, all fossil fuels will be depleted by 2088 [2]. Hence, the search for renewable energy has become extremely important over the past few years. Energy harvesting is considered a renewable energy technology and has been extensively investigated since 2006 [3]. Recently, many technologies have been employed in nanogenerators, including electromagneticity, thermoelectricity, triboelectricity, and piezoelectricity [4–7]. For example, electromagnetic generators can convert low-frequency vibrations into electrical energy via electromagnetic induction; however, they present some disadvantages such as low efficiency, heavy device weight, and high cost [8]. In addition, thermoelectric generators transform heat into electricity through the temperature gradient distribution between thermocouples. Nevertheless, a steady temperature gradient distribution is difficult to realize [9]. Triboelectric nanogenerators can generate electricity through contact and movement between material surfaces but are affected by problems of durability and warpage owing to the need of large contact size [10]. Thus, most nanogenerators cannot generate energy stably, which limits their applications in high-performance self-

* Corresponding author at: Department of Electronic Engineering, Chang Gung University, Guishan Dist. 33302, Taoyuan, Taiwan.
E-mail address: jcwang@mail.cgu.edu.tw (J.-C. Wang).

https://doi.org/10.1016/j.eurpolymj.2021.110754
Received 28 June 2021; Received in revised form 24 August 2021; Accepted 1 September 2021
Available online 4 September 2021

powered electronics [11]. In this regard, piezoelectric generators (PGs), which can generate electricity uninterruptedly through steady pressure application, are considered the most promising candidate for harvesting energy. The mainstream development of PGs is their integration with wearable devices, as well as energy harvesting by detecting human body signals to power wearable devices for realizing multiple functions [12].

Piezoelectric materials can exhibit switching dipoles when mechanical strain is applied [13]. Generally, ferroelectric materials can demonstrate piezoelectric behaviors for energy harvesting, which can primarily be categorized into two groups: inorganic (e.g., $BaTiO_3$, Pb$[Zr_xTi_{1-x}]O_3$, and $LiTaO_3$) and organic materials (e.g., poly(vinylidene fluoride) (PVDF)-based materials). Although inorganic ferroelectric materials can induce considerable polarization, they present disadvantages such as complex manufacturing processes and brittleness [4], which degrade the device performance after cyclic bending tests. Recently, organic ferroelectric materials such as PVDF and its copolymer poly(vinylidene fluoride-trifluoroethylene) (P(VDF-TrFE)) have garnered significant attention because of their advantages of high remnant polarization ($2P_r$), excellent piezoelectric response, high breakdown voltage, and high elasticity [14,15]. Under certain processing conditions, P(VDF-TrFE) can be crystallized into five phases, namely α-, β-, γ-, δ-, and ε-phases, based on different chain conformations [16,17]. In P(VDF-TrFE) copolymers, the α-phase is thermodynamically favorable but non-polar, whereas the β-phase is a polar phase that can induce strong ferro-, pyro-, and piezo-electric behaviors owing to the well-aligned polarization dipoles with the neatly arranged C-F bonds.

To achieve ferroelectricity in P(VDF-TrFE), the degree of the polar β-phase should be improved via appropriate processes such as thermal annealing, solvent vapor annealing, electrical polling, and nanofiller doping [18–21]. Among them, nanofiller doping to form nanocomposites is the simplest and most cost-effective strategy. Nanolayers, nanofibers, nanoflakes (NFs), and nanoparticles (NPs) are four types of nanofillers that can be blend with organic materials [22]. Al_2O_3 and graphene nanolayers can be inserted into the P(VDF-TrFE) films via deposition and transfer methods, respectively, as protective or transmission layers to enhance the ferroelectric behaviors of P(VDF-TrFE) for the applications in organic electronics [23,24]. For nanofibers, the main manufacturing process is electrospinning, which contributes to the enhancement of the surface-area-to-volume ratio to well-align the dipole moments in P(VDF-TrFE) copolymers [25]. Furthermore, NPs and NFs, which exhibit unique properties compared with bulk films, have been investigated extensively to improve the ferroelectric and piezoelectric characteristics of P(VDF-TrFE) copolymers. It has been reported that Au-NP and GO-NF blended P(VDF-TrFE) copolymers exhibit enhanced ferroelectric properties because of the directional arrangement of C-F bonds via the interaction between NPs/NFs and P(VDF-TrFE) copolymers [26,27]. Additionally, Wang *et al.* reported that carbon nanotubes (CNTs) can serve as a template to guide the crystal growth of P(VDF-TrFE) copolymers, and that the specific direction of CNTs enables the polarization direction to be parallel to the electric field during electrical operation, thereby improving the ferroelectric behaviors of P(VDF-TrFE) copolymers [28]. However, metal NPs and CNTs provide conductive pathways for electrons in P(VDF-TrFE) copolymers, resulting in a significant increase in leakage current that obstructs their utilization in nanogenerators [29]. In this study, n-butylamine-modified graphite nanoflakes (BMGNFs) were blended in P(VDF-TrFE) copolymers to achieve superior ferroelectric and piezoelectric properties for energy harvesting applications. Graphite is an excellent conductor owing to the sp^2 hybridization of each of its carbon atom, and its conductivity is three times higher than that of copper [30]. Graphite has been used as an electrode in ion batteries and metal–oxidesemiconductor field-effect-transistors [31,32], steel manufacturing [33], capping layers [34], and dopants in nanocomposite films [35]. The incorporation of graphite into P(VDF-TrFE) copolymers have been reported to improve the dielectric properties owing to the high conductivity of graphite [36]. In addition, it has been suggested that the graphene oxide nanosheets with high dielectric constant can be doped into P(VDF-TrFE) films to fabricate the high-performance piezoelectric nanogenerators [37]. However, the ferroelectric and piezoelectric behaviors of P(VDF-TrFE) copolymers blended with GNFs and their applications in nanogenerators have not been reported. Although the crystallization of the polar β-phase of GNF-blended P(VDF-TrFE) copolymers can be improved significantly, the high leakage current induced by GNFs worsens the ferroelectric properties. To suppress the leakage current for achieving P(VDF-TrFE) nanocomposite films with better ferroelectricity, the GNFs were modified with n-butylamine at different concentrations and then blended into P(VDF-TrFE). Subsequently, the P(VDF-TrFE)/BMGNF nanocomposites were utilized in energy harvesting devices, and the generated output power was optimized under different load resistances. The P(VDF-TrFE) copolymers blended with BMGNFs with a nitrogen percentage of 0.75 % exhibited superior ferroelectric and piezoelectric characteristics, rendering them suitable for future high-performance energy harvesting systems.

2. Experimental

2.1. Material synthesis and device preparation

Fig. 1(a) shows a schematic diagram of the BMGNF synthesis procedure. The GNF preparation method used was that proposed by Nishina *et al.* [38], and the GNFs were placed in a three-necked bottle. Two necks of the bottle were used for the injection and exhaustion of nitrogen to create an oxygen-free environment. Subsequently, n-butylamine was added at different concentrations (1 %, 10 %, and 50 %) through the remaining neck of the bottle and reacted with the GNFs. The mixed solution was dried in an ambient environment to form BMGNFs for blending in P(VDF-TrFE). The dimension (length or width) of the BMGNFs was approximately 400 nm, as confirmed via field-emission scanning electron microscopy (FE-SEM) (Fig. 1(b)), and the thickness of the BMGNFs could be approximately 3 – 5 nm according to the thickness of the flakes obtained by the electrochemical exfoliation of graphite [38]. Fig. 1(c) shows the mixing procedure for the BMGNFs and P(VDF-TrFE). Pure P(VDF-TrFE) powder (70:30 mol %) provided by Piezotech S.A.S. (Arkema, Colombes, France) and BMGNFs were dissolved in dimethylformamide, and the proportions of P(VDF-TrFE) and BMGNFs were fixed at 5 wt% and 0.01 wt%, respectively. After P(VDF-TrFE) and BMGNFs were blended, the mixing solution was stirred using a magnetic stirrer for at least 24 h to obtain a homogenous solution.

For device fabrication, a 4-inch n^+-silicon was first cleaned using the standard Radio Corporation of America cleaning procedure. To obtain uniform BMGNF-blended P(VDF-TrFE) copolymers, spin-coating was performed on the n^+-Si wafers at 1000 rpm for 30 s under a pressure of 10 Pa in N_2 ambient in a glove box. The thickness of the nanocomposite films was approximately 360 nm, which was analyzed by the ellipsometry (M−2000X, J.A. Woollam, USA). After that, the P(VDF-TrFE)/BMGNF nanocomposite films were thermally annealed at 130 °C for 2 h to enhance the crystallinity of the films, particularly that of the β-phase. Finally, a 300-nm-thick Al electrode was deposited using a thermal evaporation system at 10^{-6} Torr with a pure Al bullet (99.999% purity); subsequently, it was patterned via a standard lithographical procedure and etched using a wet solution (H_3PO_4:HNO_3:CH_3COOH:H_2O = 50:2:10:9) at 60 °C to form a top electrode. The schematic device structure of the metal–ferroelectric–metal (MFM) capacitor with the P(VDF-TrFE)/BMGNF nanocomposites is illustrated in Fig. 1(d).

2.2. Characterization of materials and devices

To identify their binding characteristics, the BMGNF-blended P(VDF-TrFE) copolymers were analyzed via X-ray photoelectron spectroscopy (XPS) (JPS-9030, JEOL, Japan) using Al Kα (1486.6 eV) radiation as the excitation source. Hence, devices with BMGNF-blended P(VDF-TrFE) copolymers are denoted as N_0.50%, N_0.75%, and N_1.00%, indicating

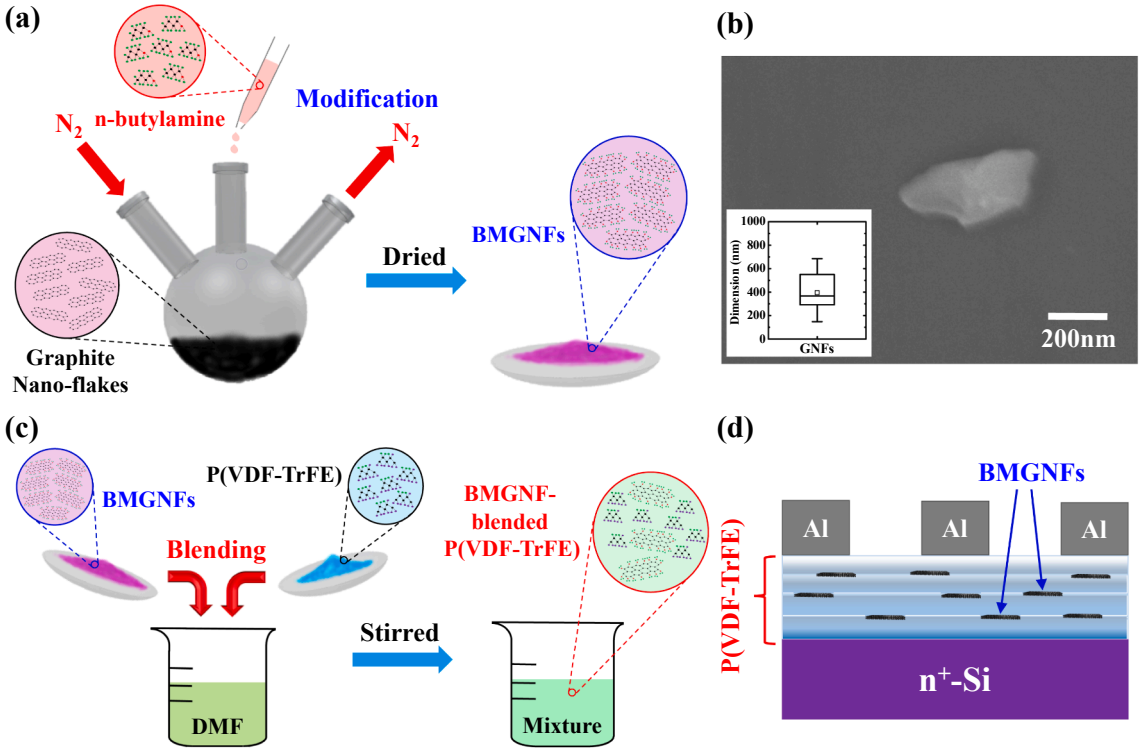

Fig. 1. (a) Schematic diagram of the BMGNF synthesis procedure. A three-necked bottle was used to modify GNFs by n-butylamine. (b) FE-SEM image of a GNF. The inset shows the statistical distribution of the dimension of GNFs. (c) Schematic diagram of the mixing procedure for the BMGNFs and P(VDF-TrFE) copolymers. The mixing solution was stirred using a magnetic stirrer for at least 24 h to obtain a homogenous solution. (d) Schematic device structure of the BMGNF-blended P(VDF-TrFE) MFM capacitor.

1 %, 10 %, and 50 % n-butylamine-modified GNFs blended in P(VDF-TrFE) copolymers, respectively, as confirmed by the atomic percentage of nitrogen from XPS spectra. Furthermore, the devices with pure P(VDF-TrFE) and GNF-blended P(VDF-TrFE) copolymers are denoted as C and G, respectively. The crystallinity of the P(VDF-TrFE)/BMGNF nanocomposite films was analyzed via X-ray diffraction (XRD) (D2 Phaser, Bruker, USA) using Cu Kα radiation and Fourier-transform infrared (FTIR) spectroscopy (Bruker Tensor 27 IR, Bruker, USA). The scanning rate and angle of incidence of the XRD analysis were 0.01° and 17–30°, respectively, and the resolution of the FTIR analysis was 2 cm^{-1}. FE-SEM (SU8010, Hitachi, Japan) and atomic force microscopy (AFM) (Digital Instruments Dimension 3100, Advanced Surface Microscopy, USA) were performed to observe the surface and cross-sectional morphologies of the P(VDF-TrFE)/BMGNF nanocomposite films. The accelerating voltage of the FE-SEM investigation was 5 kV, and the scan rate of AFM imaging was 0.5 Hz. For the electrical characterization of P(VDF-TrFE)/BMGNF MFM capacitors, the polarization vs. electric field (*P–E*) curves, leakage current density vs. electric field (*J–E*) curves, capacitance vs. electric field (*C–E*) curves, and frequency-dependent dielectric loss characteristics were analyzed using a Keithley 4200-SCS semiconductor characterization system (Tektronix Inc., USA). To investigate the energy harvesting ability of piezoelectric BMGNF-blended P(VDF-TrFE) copolymers, a high resolution digital oscilloscope (RTE1024, Rohde & Schwarz, Germany) conducted with a multichannel power probe (RT-ZVC02, Rohde & Schwarz, Germany) was used to obtain the open-circuit voltage (V_{oc}) and short-circuit current (I_{sc}) of the nanogenerators. The input resistance of the oscilloscope was 50 MΩ under the measurement of the output voltage of a nanogenerator.

3. Results and discussion

3.1. Material analyses of BMGNF-blended P(VDF-TrFE) nanocomposites

Fig. 2(a) shows the C 1 *s* and N 1 *s* XPS spectra of the BMGNF-blended P(VDF-TrFE) copolymers. In the C 1 *s* spectra, four distinct peaks located at binding energies of 286.3, 288.8, 291.0, and 292.5 eV were observed, representing the C–H, C–N/C–F, C–HF and C–F_2 bonds, respectively [39–41]. Compared with the pure P(VDF-TrFE) film, the increase in the intensity of the C–H bond for the GNF-blended and BMGNF-blended samples indicates the presence of GNFs in the P(VDF-TrFE) copolymers. Owing to the similar binding energy of approximately 288.8 eV in the XPS spectra, the C–N and C–F bonds could not be easily distinguished. Because the intensity of the C–F bond in the P(VDF-TrFE) copolymers is the same for all samples, the increase in the intensity of the C–N/C–F bonds with the nitrogen percentage of the P(VDF-TrFE)/BMGNF nanocomposites should originate from the formation of C–N bonds in the n-butylamine-modified GNFs; this can be further confirmed by the C–N bond in the N 1 *s* spectra at the binding energy of 400.8 eV [42]. It has been reported that the nitrogen-related bonds in polymers yield more insulated films [43], which significantly affect the electrical characteristics such as the leakage current of polymer films. Fig. 2(b) and (c) show the absorption spectra of FTIR in low (400–1500 cm^{-1}) and high (1500–3600 cm^{-1}) wavenumbers, respectively. In the low-wavenumber region, the peaks located at 475, 840, 1288, and 1400 cm^{-1} can be attributed to the β-phase of P(VDF-TrFE) copolymers [44,45]. The intensity of the β-phase increased as the nitrogen percentage of the nanocomposite films increased from 0.5 % to 0.75 % due to the well-aligned C–F bond and low leakage current of the film via the n-butylamine-modified GNFs. However, the crystallinity of the P(VDF-TrFE) copolymers degraded when a high concentration of n-butylamine was treated on the GNFs because the excess n-butylamine induced some unnecessary charges in the GNFs, randomized the placement of

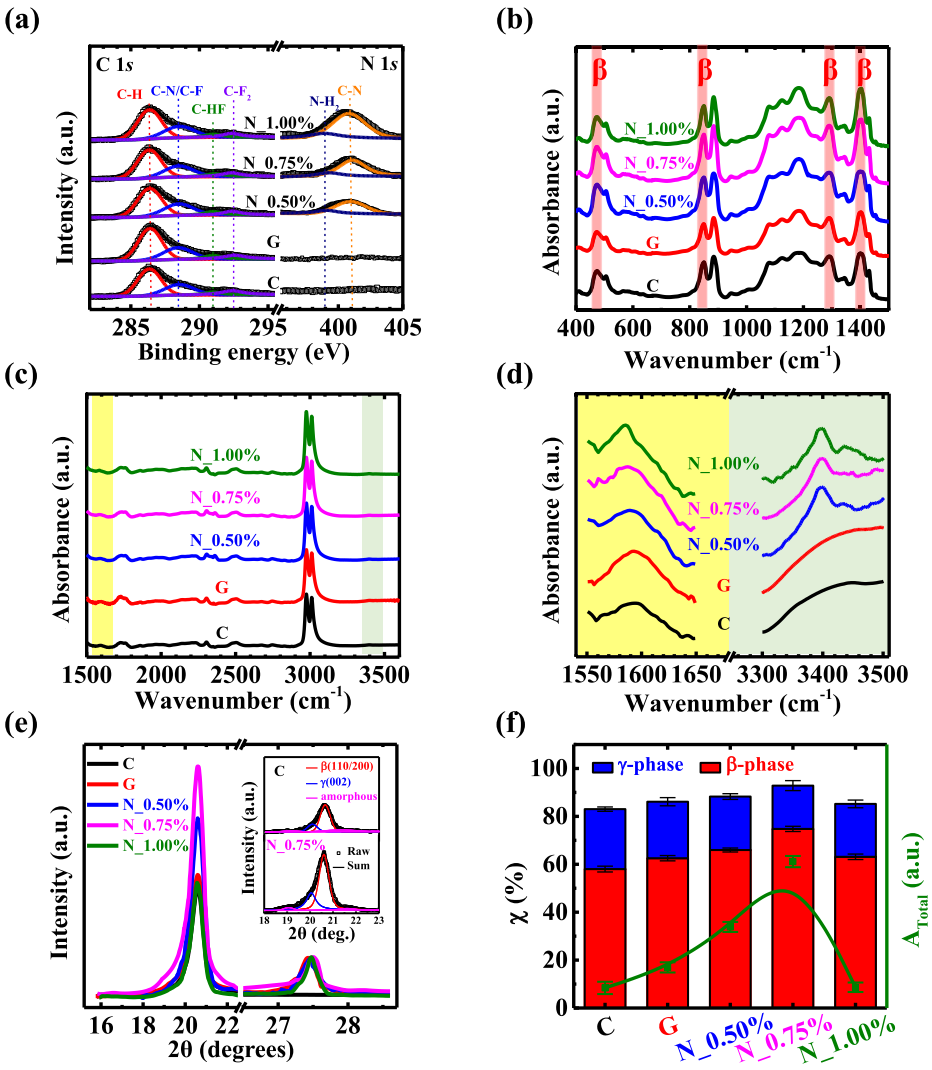

Fig. 2. (a) C 1 *s* and N 1 *s* XPS spectra of the BMGNF-blended P(VDF-TrFE) copolymers. The absorption spectra of FTIR in low (400–1500 cm^{-1}) and high (1500–3600 cm^{-1}) wavenumbers are shown in (b) and (c), respectively. (d) The enlarged spectra of the two regions marked in (c). (e) XRD patterns of the BMGNF-blended P(VDF-TrFE) copolymers. The inset shows the deconvolution in crystalline β and γ phases and non-crystalline amorphous type of XRD patterns for samples C and N_0.75%. (f) The overall crystallization area and the corresponding proportion of crystallinity of β and γ phases of the BMGNF-blended P(VDF-TrFE) copolymers.

BMGNFs, and hindered the crystallization of the films [46–48]. In the high wavenumber FTIR spectra, two important regions are noteworthy, *i.e.*, regions near 1600 cm^{-1} (Region 1, blue line) and 3400 cm^{-1} (Region 2, red line), which represent the C = C and C–N bonds, respectively [49,50]. The enlarged spectra of these two regions are presented in Fig. 2(d). In Region 1, a significant increase in the FTIR intensity at 1600 cm^{-1} can be attributed to the incorporation of GNFs in the P(VDF-TrFE) copolymers. Meanwhile, in Region 2, with the increase in the nitrogen percentage of the P(VDF-TrFE)/BMGNF nanocomposites, the FTIR intensity at 3400 cm^{-1} can be attributed to the C–N bond of the n-butylamine-modified GNFs, which was observed in the XPS spectra as well (see Fig. 2(a)).

Fig. 2(e) shows the XRD patterns of the BMGNF-blended P(VDF-TrFE) copolymers with two prominent peaks. The strong peak at 2θ = 20.5° can be attributed to the (200) and (110) reflections of the polar β-phase of the P(VDF-TrFE) copolymers. The BMGNF-blended P(VDF-TrFE) film with a nitrogen percentage of 0.75 % exhibited the highest peak, thereby demonstrating its superior polar-phase behavior. In addition, all samples showed a distinct peak at 2θ = 27.5° except for the pure P(VDF-TrFE) film. This peak reflects the crystallinity of graphite [51] and indicates the successful incorporation of GNFs into P(VDF-TrFE) copolymers. To analyze the crystallinity of the BMGNF-blended P(VDF-TrFE) copolymers, the XRD patterns were deconvoluted into three components, as shown in the inset of Fig. 2(e) and S1(b)–(d). In the deconvoluted patterns, another peak at 2θ = 20.1° was observed that belonged to the γ(002) phase [18,19,52,53], *i.e.*, a semi-polar phase between the nonpolar α- and polar β-phases. The degrees of crystallinity of the β- and γ-phases were calculated using the following equations [54]:

$$\chi_\beta = \frac{A_\beta}{A_{Total}} \times 100\% \quad (1)$$

$$\chi_\gamma = \frac{A_\gamma}{A_{Total}} \times 100\% \quad (2)$$

$$A_{total} = A_\beta + A_\gamma + A_{ams} \quad (3)$$

where A_β and A_γ are the integrated areas of the crystalline β- and γ-peaks, respectively, A_{ams} is the integrated area of the amorphous type, and A_{total} is the summation of the integrated area of all diffraction peaks. The calculated values of A_{total} and the proportion of crystallinity of the β- and γ-phases of the BMGNF-blended P(VDF-TrFE) copolymers are shown in Fig. 2(f). For the pure P(VDF-TrFE) film, the degrees of crystallinity of the β- and γ-phases were only 58.01 % and 25.03 %, respectively. For the P(VDF-TrFE) copolymers blended with BMGNFs, the overall crystallization area, *i.e.*, the summation of the crystallinity of the β-phase (χ_β) and γ-phase (χ_γ), increased significantly. In addition, the transformation from the γ-phase to the β-phase became more significant when the nitrogen percentage of the BMGNFs increased to 0.75 %, *i.e.*, χ_β increased to 74.77 %, whereas χ_γ decreased to 18.07 %. It was evident

that the phase transformation was owing to the good alignment of the C–F bond and the low leakage current of the film via the modified GNFs, as revealed in the FTIR spectra of Fig. 2(b)–(d). However, for the P(VDF-TrFE)/BMGNF nanocomposites with a nitrogen percentage of 1 %, the overall crystallization area attenuated to 85.21 %, and the phase transformation was vague, which can be ascribed to crystallization hindrance by the excess n-butylamine modification in the GNFs.

Fig. 3(a),(b) and S2 show the surface morphologies of the P(VDF-TrFE)/BMGNF nanocomposites. Compared with the samples without GNFs, the P(VDF-TrFE) copolymers blended with BMGNFs, *i.e.* sample N_0.75%, presented a significant needle-shaped crystalline structure, indicating that the crystallization of the polar β-phase can be enhanced through the blending of BMGNFs. If the amount of n-butylamine modification in the GNFs is increased to 50 %, *i.e.* sample N_1.00%, then fewer needle-shaped crystalline structures will be observed in the P(VDF-TrFE) copolymers, which can be ascribed to the crystallization hindrance by the excess n-butylamine modification in the GNFs. The needle-like crystallization of the β-phase in the P(VDF-TrFE)/BMGNF nanocomposites can be further confirmed by the FE-SEM topographic images, as shown in Fig. 3(c),(d) and S3(a)–(c). As shown in Fig. 3(d), the crystal length of needles in the P(VDF-TrFE)/BMGNF nanocomposites was defined [55]. To obtain a statistical distribution, more than 100 needles for each sample were measured, as plotted in Fig. S3(d). When the amount of n-butylamine modified in the GNFs increased to 10 % (sample N_0.75%), the average crystal length of the needles in the P(VDF-TrFE)/BMGNF nanocomposites increased from 295.7 to 682.4 nm, resulting in an enhanced crystallization of the polar β-phase. Nevertheless, the excessive n-butylamine modification in the GNFs led to a decrease in the crystal length of the needles to 283.7 nm for the low crystallization of the β-phase in the P(VDF-TrFE)/BMGNF nanocomposites, which is consistent with the AFM images. Fig. 3(e) and (f) show the cross-sectional FE-SEM images of the pure and BMGNF-blended P(VDF-TrFE) nanocomposites, respectively, for analyzing the placement of BMGNFs in P(VDF-TrFE). For the P(VDF-TrFE) blended with BMGNFs, the BMGNFs were placed horizontally in the P(VDF-TrFE) copolymers, contributing to well-aligned C–F bonds by the interaction between the BMGNFs and P(VDF-TrFE) for enhanced ferroelectric behaviors, which will be discussed later.

3.2. *Electrical behaviors of ferroelectric MFM capacitors with BMGNF-blended P(VDF-TrFE) copolymers*

A schematic illustration of the crystallite structures of the P(VDF-TrFE)/BMGNF nanocomposites are illustrated in Fig. 4. For the pure P(VDF-TrFE) copolymers, a thermodynamically unstable α-phase and randomly aligned dipoles were observed (Fig. 4(a)), which resulted in a low amount of polar β-phase in the P(VDF-TrFE) copolymers [56]. To enhance the ferroelectric behaviors, the GNFs were blended into P(VDF-TrFE) to achieve well-aligned polarization dipoles, as shown in Fig. 4(b). However, the highly conductive GNFs might induce conductive pathways in the P(VDF-TrFE) copolymers. Therefore, the GNFs were modified with n-butylamine and then blended into P(VDF-TrFE) copolymers in this study. For the P(VDF-TrFE) copolymers blended with moderate n-butylamine modified GNFs, *i.e.*, sample N_0.75%, not only the polarization dipoles were arranged neatly via GNFs, but also the GNFs were modified by the amino groups (Fig. 4(c)). In XPS and FTIR spectra (Fig. 2(a) and (d)), the amino groups at BMGNFs of the P(VDF-TrFE)/BMGNF nanocomposite films were observed, thereby inducing the positive

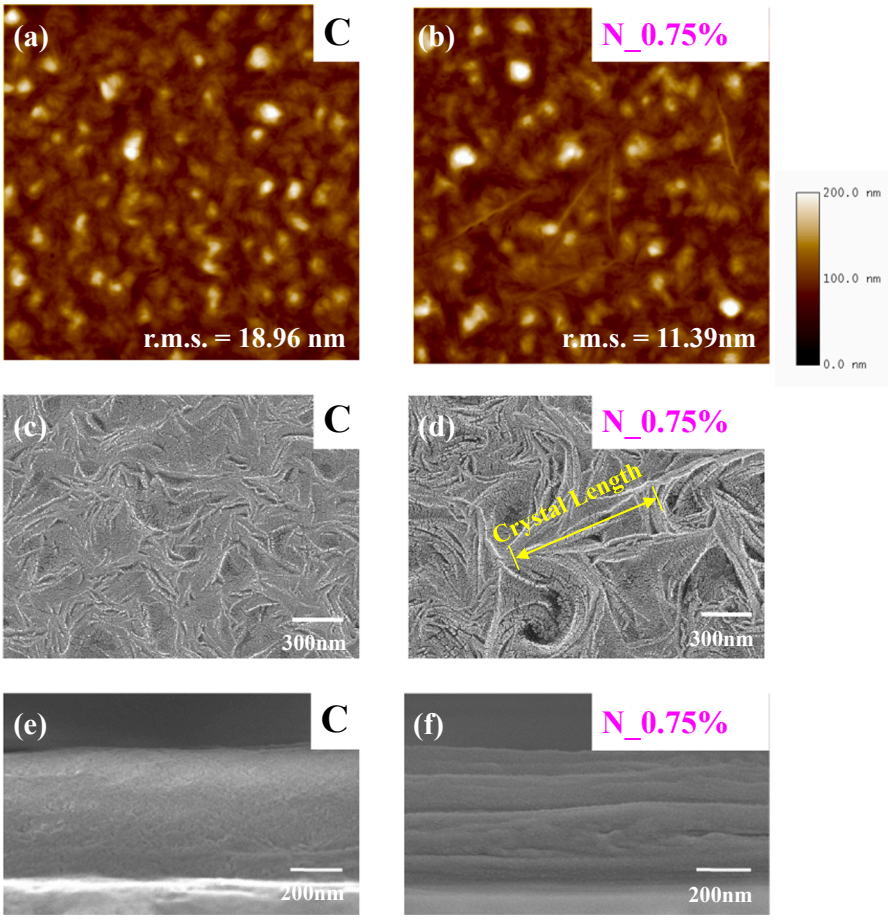

Fig. 3. AFM surface morphologies of (a) pure (VDF-TrFE) and (b) P(VDF-TrFE)/BMGNF nanocomposites with a nitrogen percentage of 0.75 %. FE-SEM topographic and cross-sectional images of (c),(e) pure (VDF-TrFE) and (d),(f) P(VDF-TrFE)/BMGNF nanocomposites with a nitrogen percentage of 0.75 %, respectively.

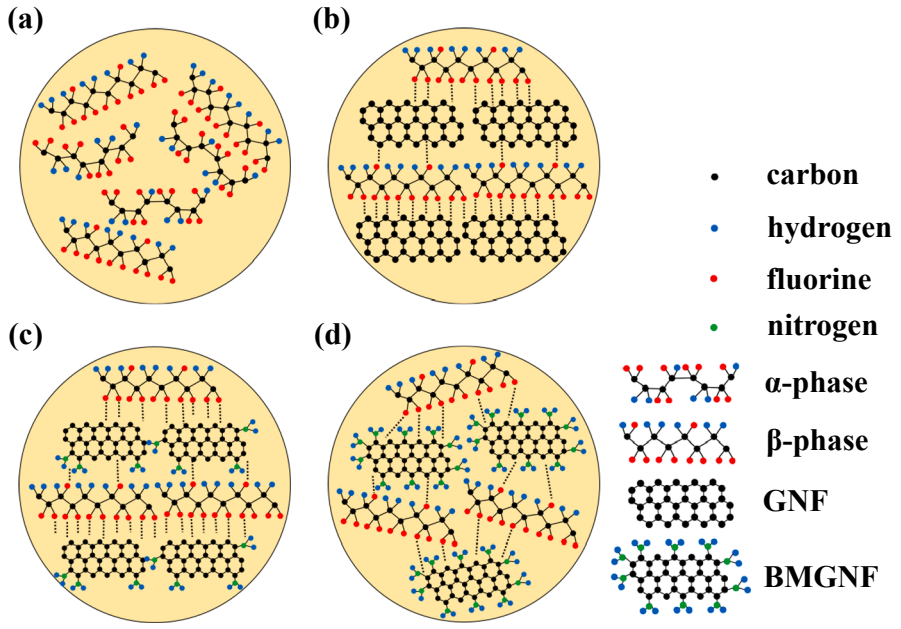

Fig. 4. Schematic crystallite structures of (a) pure P(VDF-TrFE), (b) GNF-blended P(VDF-TrFE), and BMGNF-blended P(VDF-TrFE) nanocomposites with a nitrogen percentage of (c) 0.75 % and (d) 1 %.

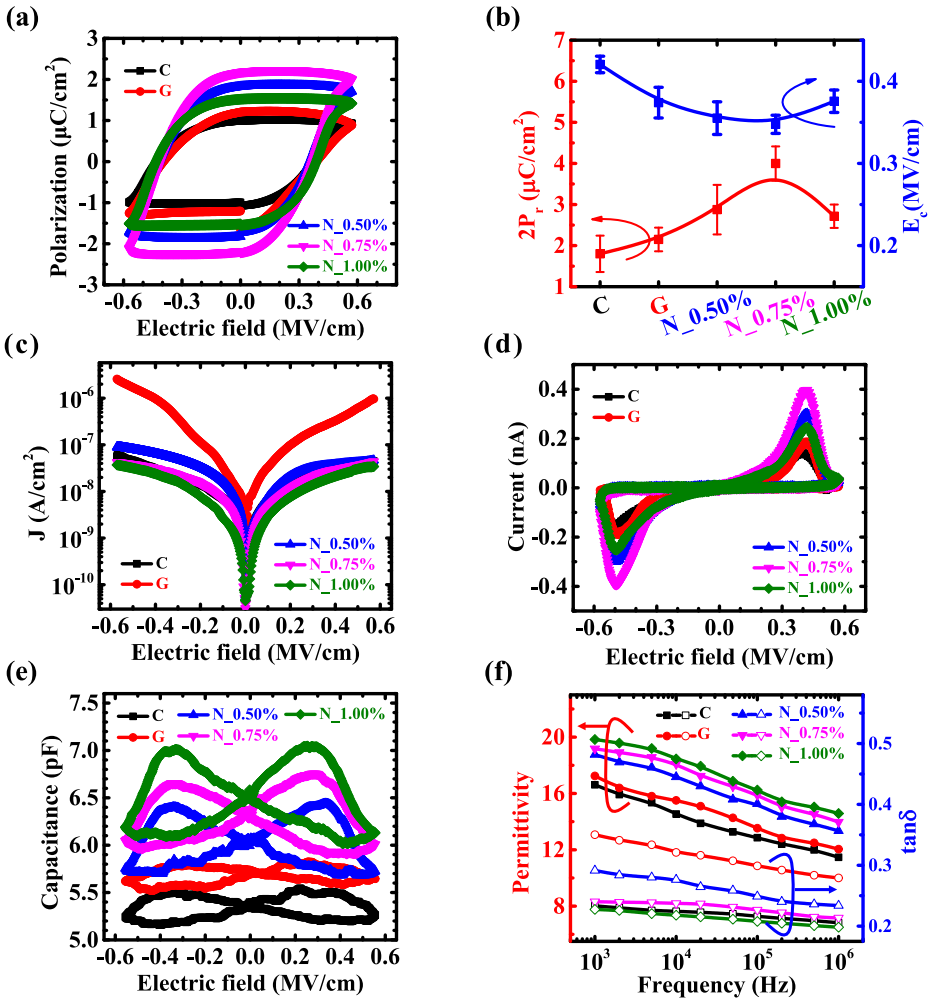

Fig. 5. (a) *P–E* characteristics, (b) statistical distributions of $2P_r$ and E_c, (c) leakage current density, (d) *I–E* characteristics, (e) *C–E* characteristics, and (f) relative permittivity and dielectric loss vs. frequency characteristics of the BMGNF-blended P(VDF-TrFE) MFM capacitors.

charges at the amino terminus [46,47]. The large number of positive charges generated by the excessive n-butylamine modification in the GNFs randomized the placement of BMGNFs and interfered with the alignment of the polar β-phase in the P(VDF-TrFE) copolymers [48], as shown in Fig. 4(d), giving rise to the degradation of ferroelectric characteristics.

To characterize the ferroelectric behaviors of the BMGNF-blended P(VDF-TrFE) MFM capacitors, all devices were measured using the positive-up negative-down (PUND) method [57] with an applied bias of ± 20 V at a frequency of 20 Hz. Fig. 5(a) shows the *P–E* characteristics of all samples. At least 10 devices of each sample were measured to investigate the effect of the BMGNF-blended P(VDF-TrFE) on the ferroelectric properties. The statistical distributions of $2P_r$ and E_c were extracted, as shown in Fig. 5(b). For the MFM capacitors with GNF-blended P(VDF-TrFE) nanocomposites, *i.e.*, sample G, only a slight increase in $2P_r$ was observed. By contrast, when the GNFs were modified with n-butylamine and blended into the P(VDF-TrFE) copolymers, a significant improvement in the *P–E* curves of the MFM capacitors was obtained. When the nitrogen percentage of the P(VDF-TrFE)/BMGNF nanocomposites increased to 0.75 %, the $2P_r$ increased to more than 4 μC/cm^2 and the E_c reduced to less than 0.35 MV/cm owing to the well-aligned polarization dipoles by the interaction between the BMGNFs and P(VDF-TrFE) copolymers, as illustrated in Fig. 4(c). Compared with the samples with P(VDF-TrFE)/BMGNF nanocomposites, sample G showed a worse ferroelectric behaviors because of the high leakage current originating from the undesirable conducting paths through the GNFs [36], as shown in Fig. 5(c). On the other hand, for the samples with excessive n-butylamine modification in the GNFs, *i.e.*, sample N_1.00%, the ferroelectric behaviors worsened because the large number of positive charges at the amino terminus induced by the excess n-butylamine modification in the GNFs disrupted the arrangement of dipoles in the P(VDF-TrFE) copolymers, as displayed in Fig. 4(d). Fig. 5(d) shows the *J–E* hysteresis loops of all samples. A significant increase in the switching current of the capacitors with P(VDF-TrFE)/BMGNF nanocomposites was achieved, which is consistent with the characteristics exhibited by the *P–E* curves. To further confirm the effects of the BMGNFs blended in the P(VDF-TrFE) copolymers, the *C–E* characteristics of the MFM capacitors at a frequency of 1 MHz were analyzed, as shown in Fig. 5(e). All samples exhibited butterfly-shaped hysteresis loops, indicating ferroelectric polarization. It is noteworthy that the capacitance of the devices with GNF- and BMGNF-blended P(VDF-TrFE) nanocomposites increased significantly, which can be ascribed to the enhancement in permittivity via graphite incorporation [36] and additional n-butylamine modification in the GNFs [58]. The frequency dispersion characteristics of the MFM capacitors with P(VDF-TrFE)/BMGNF nanocomposites were analyzed at frequencies ranging from 1 kHz to 1 MHz at a bias of 20 V, as shown in Fig. 5(f). As the frequency increased, both the relative permittivity and dielectric loss (tanδ) of all samples decreased gradually due to the delayed response of the space charges and dipole moments in the P(VDF-TrFE) films under the high switching speed of an external electric field [59,60]. At the high-frequency operation, the polarizations of the space charges and dipole moments decrease and the corresponding charges can only execute a localized motion, resulting in a reduced permittivity and dielectric loss, respectively. Compared with other samples, a high dielectric loss of the MFM capacitors with GNF-blended P(VDF-TrFE) nanocomposites was observed, which can be ascribed to the high leakage current, as presented in Fig. 5(c). By contrast, the dielectric loss can be effectively reduced by the n-butylamine modification in the GNFs, which is suitable for applications in energy harvesting.

3.3. Output characteristics of piezoelectric nanogenerators with BMGNF-blended P(VDF-TrFE) copolymers

To investigate the piezoelectric energy harvesting behaviors of the P(VDF-TrFE)/BMGNF nanocomposites, the output voltage was measured under different applied pressures (19.6–78.4 kPa) at a frequency of 7 Hz. Fig. 6(a),(b) and S4 show the open-circuit output voltages generated by the BMGNF-blended P(VDF-TrFE) nanogenerators. In these figures, a strong correlation between the pressures and the peak output voltages was observed, demonstrating the superb piezoelectric behavior of the P(VDF-TrFE) copolymers. The peak output voltages of the samples under different applied pressures were extracted, as shown in Fig. 6(c). For the BMGNF-blended P(VDF-TrFE) nanogenerators with a nitrogen percentage of 0.75 %, a peak output voltage of 4.9 V was obtained under an applied pressure of 78.4 kPa, which was approximately twice larger than that of the pure P(VDF-TrFE). The outstanding energy harvesting capability of sample N_0.75% can be ascribed to its superior ferroelectric characteristics, as shown in Fig. 4. To acquire the short-circuit output current of the BMGNF-blended P(VDF-TrFE) nanogenerators, a multi-channel power probe was connected to the oscilloscope. Figs. S5(a)–(e) show the output currents of the samples under different applied pressures. Similarly, all samples generated currents stably, and the highest output current of 4.5 μA was achieved in sample N_0.75% under an applied pressure of 78.4 kPa, as shown in Fig. S5(f). According to the literature [11], the power density of a nanogenerator is important for evaluating its energy-harvesting performance. Fig. 6(d) illustrates a schematic diagram of the measurement setup to obtain the power density of a nanogenerator, where a load resistance was applied across the nanogenerator, and an oscilloscope was used to record the output voltage. A real image of the measurement system is also presented in Fig. S6. To obtain the maximum power density and extract the internal resistance of the BMGNF-blended P(VDF-TrFE) nanogenerators simultaneously, the load resistances were varied from 0.5 to 20 MΩ. Fig. 6(e), (f) and S7(a)–(c) show the output voltages of all samples under a repetitive and compressive cycling pressure of 78.4 kPa. The output voltage as a function of the load resistance was measured, as shown in Fig. S7(d). Subsequently, the power density (S) can be calculated using the following equation:

$$S = \frac{V_{out}^2}{R_L} \tag{4}$$

where R_L is the load resistance and V_{out} is the output voltage across R_L. Fig. 6(g) shows the power density vs. load resistance characteristics of the BMGNF-blended P(VDF-TrFE) nanogenerators. When the nitrogen percentage increased to 0.75 %, the power density enhanced significantly. The maximum power density of sample N_0.75% was approximately 33.73 mW/m^2, which was more than three times higher than that of the pure P(VDF-TrFE) devices. However, for the P(VDF-TrFE)/BMGNF nanocomposites with the excessive n-butylamine modification (sample N_1.00%), the power density decreased significantly. If an internal resistance in series with the voltage across the piezoelectric film is used to model a P(VDF-TrFE) nanogenerator [9], as illustrated in Fig. 6(d), then the internal resistance (R_i) can be calculated using the following equation:

$$R_i = \left(\frac{V_p}{V_{out}} - 1\right) \times V_{out} \times R_L \tag{5}$$

where V_p is the voltage across the piezoelectric films. Fig. 6(h) shows the internal resistance vs. load resistance characteristics of the BMGNF-blended P(VDF-TrFE) nanogenerators. Compared with the pure P(VDF-TrFE), a smaller internal resistance of 1.5 and 1.8 MΩ was observed in samples N_0.50% and N_0.75%, respectively, indicating that the generated output voltage can be delivered much more easily to the load resistance for better power generation efficiency. For a material with superior ferroelectric properties and a low internal resistance, *i.e.*, sample N_0.75%, as shown in Fig. 4(a) and 6(h), the power generation efficiency of a nanogenerator would be better and more suitable for further integration in application-specific integrated circuits. Finally, a cycling test was performed to confirm the stability of the BMGNF-blended P(VDF-TrFE) nanogenerators with a nitrogen percentage of

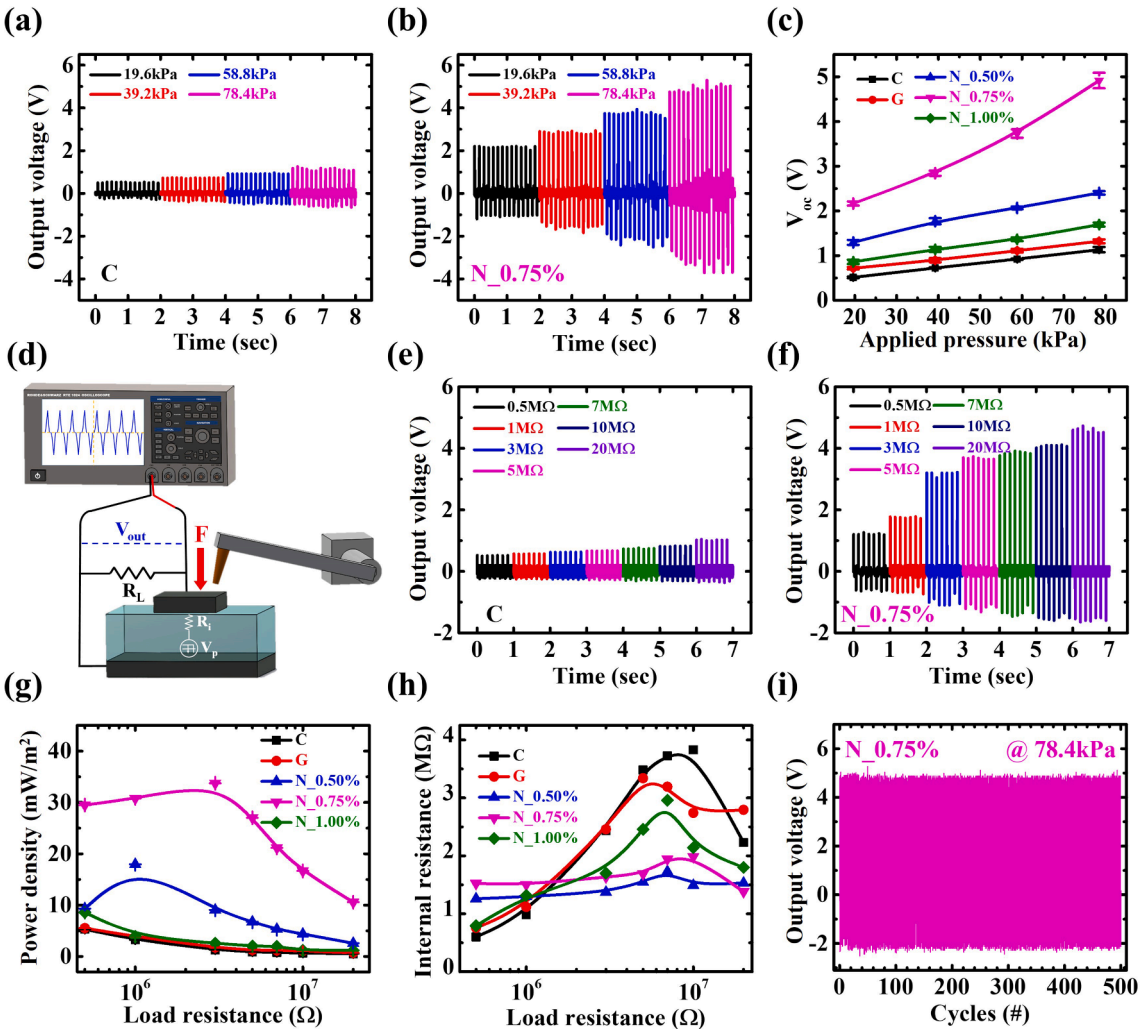

Fig. 6. Output voltage characteristics of (a) pure P(VDF-TrFE) and (b) BMGNF-blended P(VDF-TrFE) nanogenerators with a nitrogen percentage of 0.75 % under different applied pressures at 7 Hz. (c) Statistical distributions of the open-circuit voltage for the BMGNF-blended P(VDF-TrFE) nanogenerators under different applied pressures. (d) Measurement setup of the energy harvesting system with a load resistance in parallel with the P(VDF-TrFE) nanogenerator. An internal resistance in series with the voltage across the piezoelectric film is used to model a P(VDF-TrFE) nanogenerator. Output voltage characteristics of (e) pure P(VDF-TrFE) and (f) BMGNF-blended P(VDF-TrFE) nanogenerators with a nitrogen percentage of 0.75 % under an applied pressure of 78.4 kPa at different load resistances. (g) Power density and (h) internal resistance vs. load resistance characteristics of the BMGNF-blended P(VDF-TrFE) nanogenerators. (i) Cycling test of the BMGNF-blended P(VDF-TrFE) nanogenerators with a nitrogen percentage of 0.75 % under an applied pressure of 78.4 kPa.

0.75 %, as shown in Fig. 6(i). The applied pressure was fixed at 78.4 kPa during the testing. The results show that the generated output voltage was stable over 500 cycles, meaning the potential of the nanogenerators fabricated using P(VDF-TrFE)/BMGNF nanocomposites for future self-powered consumer electronics. Table S1 summarizes the output performances of the piezoelectric nanogenerators of this study and some published works. Compared with other materials, the BMGNF-blended P(VDF-TrFE) copolymers show competitive performances of output voltage, output current, and power density in piezoelectric energy harvesting.

4. Conclusion

In this work, it was demonstrated that the excellent crystalline structure and superior ferroelectric properties of the P(VDF-TrFE)/BMGNF nanocomposites resulted in piezoelectric nanogenerators with high power generation efficiency. XPS, FTIR, and XRD were performed to confirm the blending of BMGNFs in P(VDF-TrFE) and the transformation from the γ-phase to β-phase of P(VDF-TrFE) copolymers through the blending of BMGNFs. By analyzing the FE-SEM and AFM images, a needle-shaped crystalline structure was observed in the BMGNF-blended P(VDF-TrFE) copolymers. Furthermore, it was observed that the BMGNFs were placed horizontally in the P(VDF-TrFE) copolymers, leading to well-aligned polarization dipoles because of the interaction between BMGNFs and P(VDF-TrFE), and enhanced ferroelectric behaviors indicated by a high $2P_r$ of more than 4 μC/cm^2 and a low E_c of less than 0.35 MV/cm. With an appropriate n-butylamine modification in the GNFs, the dielectric loss induced by the leakage current of the P(VDF-TrFE) copolymers decreased significantly owing to the reduction in the conductive pathways of electrons through the GNFs, resulting in excellent ferroelectric behaviors. Therefore, the P(VDF-TrFE)/BMGNF nanocomposites were utilized in piezoelectric nanogenerators to yield a high output voltage of 4.9 V, a high output current of 4.5 μA, and a high generating power density of 33.73 mW/m^2 under an applied pressure of 78.4 kPa. The BMGNF-blended P(VDF-TrFE) nanogenerators can convert mechanical energy to electrical signals effectively without any degradation for more than 500 cycles; hence, they are a promising candidate for future high-performance organic sensors and self-powered consumer electronics.

CRediT authorship contribution statement

Tzu-Chuan Yang: Investigation, Validation, Data curation, Writing – original draft. **Yi-Pei Jiang:** Investigation, Validation. **Ting-Han Lin:** Investigation. **Shih-Hsuan Chen:** Investigation. **Ching-Mei Ho:** Investigation. **Ming-Chung Wu:** Methodology, Resources. **Jer-Chyi Wang:** Conceptualization, Methodology, Writing – review & editing, Supervision.

Declaration of Competing Interest

The authors declare that they have no known competing financial interests or personal relationships that could have appeared to influence the work reported in this paper.

Acknowledgements

This research was supported by Ministry of Science and Technology, R.O.C. (Contract No. of MOST 109-2221-E-182-032) and Chang Gung Memorial Hospital, Linkou, Taiwan (Contract Nos. of CMRPD2H0133, CMRPD2J0052, and BMRPA74).

Data availability statement

The raw/processed data required to reproduce these findings cannot be shared at this time as the data also forms part of an ongoing study.

Appendix A. Supplementary data

Supplementary data to this article can be found online at https://doi.org/10.1016/j.eurpolymj.2021.110754.

Reference

[1] H. Ritchie, M. Roser (2020) - "Energy". Published online at OurWorldInData.org. Retrieved from: https://ourworldindata.org/energy.
[2] A. Kalair, N. Abas, M.S. Saleem, A.R. Kalair, N. Khan, Role of energy storage systems in energy transition from fossil fuels to renewables, Energy Storage 3 (2020) e. 135.
[3] Z.L. Wang, J. Song, Piezoelectric nanogenerators based on zinc oxide nanowire arrays, Science 312 (2006) 242–246.
[4] A. Sultana, S.K. Ghosh, M.M. Alam, P. Sadhukhan, K. Roy, M. Xie, C.R. Bowen, S. Sarkar, S. Das, T.R. Middya, D. Mandal, Methylammonium lead iodide incorporated poly(vinylidene fluoride) nanofibers for flexible piezoelectric−pyroelectric nanogenerator, ACS Appl. Mater. Interfaces 11 (2019) 27279–27287.
[5] S. Zhu, C. Liu, K. Wang, Y. Hu, Y. Ning, Theoretical and experimental analyses of a hybrid excitation synchronous generator with integrated brushless excitation, IET Electr. Power Appl. 10 (2016) 258–267.
[6] J.-H. Zhang, Y. Li, J. Du, H. Huang, A high-power wearable triboelectric nanogenerator prepared from self-assembled electrospun poly(vinylidene fluoride) fibers with a heart-like structure, J. Mater. Chem. A 7 (2019) 11724–11733.
[7] S. Hu, S. Zeng, X. Li, J. Jiang, W. Yang, Y. Chen, M. Li, J. Zheng, Flexible and high performance of n-type thermoelectric PVDF compositefilm induced by nickel nanowires, Mater. Des. 188 (2020), 108496.
[8] Hassan Askari, Amir Khajepour, Mir Behrad Khamesee, Zia Saadatnia, Zhong Lin Wang, Piezoelectric and triboelectric nanogenerators: Trends and impacts, Nano Today 22 (2018) 10–13.
[9] Ayesha Sultana, M.M. Alam, Tapas Ranjan Middya, Dipankar Mandal, A pyroelectric generator as a self-powered temperature sensor for sustainable thermal energy harvesting from waste heat and human body heat, Appl. Energy 221 (2018) 299–307.
[10] A. Gaur, S. Tiwari, C. Kumar, P. Maiti, A bio-based piezoelectric nanogenerator for mechanical energy harvesting using nanohybrid of poly(vinylidene fluoride), Nanoscale Adv. 1 (2019) 3200–3211.
[11] Y. Wang, Y. Yang, Z.L. Wang, Triboelectric nanogenerators as flexible power sources, npj Flex, Electron. 1 (2017) 10.
[12] X. Chen, X. Li, J. Shao, N. An, H. Tian, C. Wang, T. Han, L. Wang, B. Lu, High-performance piezoelectric nanogenerators with imprinted P(VDF-TrFE)/$BaTiO_3$ nanocomposite micropillars for self-powered flexible sensors, Small 13 (2017) 1604245.
[13] Keun Young Lee, Dohwan Kim, Ju-Hyuck Lee, Tae Yun Kim, Manoj Kumar Gupta, Sang-Woo Kim, Unidirectional high-power generation via stress-induced dipole alignment from $ZnSnO_3$ nanocubes/polymer hybrid piezoelectric nanogenerator, Adv. Funct. Mater. 24 (1) (2014) 37–43.
[14] Lu Yang, Qiuying Zhao, Ying Hou, Rujie Sun, Meng Cheng, Mingxia Shen, Shaohua Zeng, Hongli Ji, Jinhao Qiu, High breakdown strength and outstanding piezoelectric performance inflexible PVDF based percolative nanocomposites through the synergisticeffect of topological-structure and composition modulations, Compos. Part A Appl. Sci. Manuf. 114 (2018) 13–20.
[15] Fu-Chang Sun, Avinash M. Dongare, Alexandru D. Asandei, S. Pamir Alpay, Serge Nakhmanson, X Temperature dependent structural, elastic, and polar properties of ferroelectric polyvinylidene fluoride (PVDF) and trifluoroethylene (TrFE) copolymers, J. Mater. Chem. C 3 (32) (2015) 8389–8396.
[16] Nan Jia, Qian He, Jing Sun, Guangmei Xia, Rui Song, Crystallization behavior and electroactive properties of PVDF, P(VDF-TrFE) and their blendfilms, Polym. Test. 57 (2017) 302–306.
[17] S.-W. Hahm, D.-Y. Khang, Crystallization and microstructure-dependent elastic moduli of ferroelectric P(VDF–TrFE) thin films, Soft Matter 6 (2010) 5802.
[18] Y.P. Jiang, T.C. Yang, T.H. Lin, C.M. Ho, S.H. Chan, M.C. Wu, J.C. Wang, Layer-dependent solvent vapor annealing on stacked ferroelectric P(VDF-TrFE) copolymers for highly efficient nanogenerator applications, Polymer 204 (2020), 122822.
[19] Weimin Xia, Zhigang Wang, Junhong Xing, Congjun Cao, Zhuo Xu, The dependence of dielectric and ferroelectric properties on crystal phase structures of the hydrogenized P(VDF-TrFE) films with different thermal processing, IEEE Trans. Ultrason. Ferroelectr. Freq. Control 63 (10) (2016) 1674–1680.
[20] A. Hartono, Darwin, Ramli, S. Satira, M. Djamal, Herman, Electric field poling 2G V/m to improve piezoelectricity of PVDF thin film, AIP Conf. Proc. 1719 (2016) 030021.
[21] H. Paik, Y.Y. Choi, S. Hong, K. No, Effect of Ag nanoparticle concentration on the electrical and ferroelectric properties of Ag/P(VDF-TrFE) composite films, Sci. Rep. 5 (2015) 13209.
[22] Iman Harsini, Muhammad Maqbool Sadiq, Parviz Soroushian, Anagi M. Balachandra, Polymer nanocomposites processed via self-assembly through introduction of nanoparticles, nanosheets, and nanofibers, J. Mater. Sci. 52 (4) (2017) 1969–1980.
[23] Chan Ho Park, Kwang H. Lee, Byoung H. Lee, Myung M. Sung, Seongil Im, Channel/ferroelectric interface modification in ZnO non-volatile memory TFT with P(VDF-TrFE) polymer, J. Mater. Chem. 20 (13) (2010) 2638–2643.
[24] Sang-Hoon Bae, Orhan Kahya, Bhupendra K. Sharma, Junggou Kwon, Hyoung J. Cho, Barbaros Özyilmaz, Jong-Hyun Ahn, Graphene-P(VDF-TrFE) multilayer film for flexible applications, ACS Nano 7 (4) (2013) 3130–3138.
[25] Chang-Chun Wang, Jiao-Fan Song, Hui-Min Bao, Qun-Dong Shen, Chang-Zheng Yang, Enhancement of electrical properties of ferroelectric polymers by polyaniline nanofibers with controllable conductivities, Adv. Funct. Mater. 18 (8) (2008) 1299–1306.
[26] N. Tsutsumi, R. Kosugi, K. Kinashi, W. Sakai, Nature of the enhancement in ferroelectric properties by gold nanoparticles in vinylidene fluoride and trifluoroethylene copolymer, ACS Appl. Mater. Interfaces 8 (2016) 16816–16822.
[27] R.M. Habibur, U. Yaqoob, S. Muhammad, A.S.M.I. Uddin, H.C. Kim, The effect of RGO on dielectric and energy harvesting properties of P(VDF-TrFE) matrix by optimizing electroactive β phase without traditional polling process, Mater. Chem. Phys. 215 (2018) 46–55.
[28] M. Wang, L. Li, S. Zhou, R. Tang, Z. Yang, X. Zhang, Influence of CNTs on the crystalline microstructure and ferroelectric behavior of P(VDF-TrFE), Langmuir 34 (2018) 10702–10710.
[29] M. Zhao, Q. Fu, Y. Hou, L. Luo, W. Li, $BaTiO_3$/MWNTs/polyvinylidene fluoride ternary dielectric composites with excellent dielectric property, high breakdown strength, and high-energy storage density, ACS Omega 4 (2019) 1000–1006.
[30] L. Pietronero, S. Strassler, H.R. Zeller, M.J. Rice, Electrical conductivity of a graphite layer, Phys. Rev. B 22 (1980) 904.
[31] X. Zhang, Y. Tang, F. Zhang, C.S. Lee, A novel aluminium-graphite dual-ion battery, Adv. Energy Mater. 6 (2016) 1502588.
[32] K. Bhatt, C. Rani, M. Vaid, A. Kapoor, P. Kumar, S. Kumar, S. Shriwastawa, S. Sharma, R. Singh, C.C. Tripathi, A comparative study of graphene and graphite-based field effect transistor on flexible substrate, Pramana 90 (2018) 75.
[33] Steven D. Machemer, Characterization of airborne and bulk particulate from iron and steel manufacturing facilities, Environ. Sci. Technol. 38 (2) (2004) 381–389.
[34] Harsh Naik, K. Tang, T. Paul Chow, Effect of graphite cap for implant activation on inversion channel mobility in 4H-SiC MOSFETs, Mater. Sci. Forum 615-617 (2009) 773–776.
[35] L.G.P. Tienne, T.B. de Abreu, F.F. Gondim, B.D.S.M. da Cruz, G.R. Martins, R. A. Simão, M.D.F.V. Marques, Low contents of graphite improving general properties of poly(vinylidene fluoride), Polym. Test. 91 (2020), 106790.
[36] X. Li, X. Wang, L. Weng, Y. Yu, X. Zhang, L. Liu, C. Wang, Dielectrical properties of graphite nanosheets/PVDF composites regulated by coupling agent, Mater. Today Commun. 21 (2019), 100705.
[37] Yunqiu Wang, Minjie Fang, Bobo Tian, Pinghua Xiang, Ni Zhong, Hechun Lin, Chunhua Luo, Hui Peng, Chun-Gang Duan, Transparent PVDF-TrFE/graphene oxide ultrathin films with enhanced energy harvesting performance, ChemistrySelect 2 (26) (2017) 7951–7955.
[38] H. Hashimoto, Y. Muramatsu, Y. Nishina, H. Asoh, Bipolar anodic electrochemical exfoliation of graphite powders, Electrochem. Commun. 104 (2019), 106475.
[39] Jer-Chyi Wang, Yi-Pei Jiang, Yu-Jie Lin, Shun-Hsiang Chan, Ming-Chung Wu, Trifluoroethylene bond enrichment in P(VDF-TrFE) copolymers with enhanced ferroelectric behaviors by plasma fluorination on bottom electrode, J. Taiwan Inst. Chem. Eng. 107 (2020) 152–160.
[40] B. Xu, C.N. Borca, S. Ducharme, A.V. Sorokin, P.A. Dowben, V.M. Fridkin, S. P. Palto, N.N. Petukhova, S.G. Yudin, Aluminum doping of poly(vinylidene fluoride with trifluoroethylene) copolymer, J. Chem. Phys. 114 (2001) 1866–1869.

[41] J.J. Li, W.T. Zheng, H.H. Wu, L. Sun, G.G. Gu, H.J. Bian, X.Y. Lu, Z.S. Jin, Compositional and structural modifications of amorphous carbon nitride films induced by thermal annealing, J. Phys. D Appl. Phys. 36 (2003) 2001–2005.
[42] S.S. Shinde, A. Samia, J.-H. Lee, Electrocatalytic hydrogen evolution using graphitic carbon nitride coupled with nanoporous graphene co-doped by S and Se, J. Mater. Chem. A 3 (2015) 12810–12819.
[43] Atsushi Masuda, Hironobu Umemoto, Hideki Matsumura, Various applications of silicon nitride by catalytic chemical vapordeposition for coating, passivation and insulating films, Thin Solid Films 501 (1-2) (2006) 149–153.
[44] G. Suresh, G. Mallikarjunachari, S. Jatav, C. Thirmal, M.S.R. Rao, D.K. Satapathy, Evolution of morphology, ferroelectric, and mechanical properties in poly (vinylidene fluoride)–poly(vinylidene fluoride-trifluoroethylene) blends, J. Appl. Polym. Sci. 135 (2018) 45955.
[45] Xiaomei Cai, Tingping Lei, Daoheng Sun, Liwei Lin, A critical analysis of the α, β and γ phases in poly(vinylidene fluoride) using FTIR, RSC Adv. 7 (25) (2017) 15382–15389.
[46] M. Akita, S. Sasaki, S. Matsuyama, S. Mizushima, SecA interacts with secretory proteins by recognizing the positive charge at the amino terminus of the signal peptide in Escherichia coli, J. Biol. Chem. 265 (14) (1990) 8164–8169.
[47] M. Morpurgo, C. Monfardini, L.J. Hofland, M. Sergi, P. Orsolini, J.M. Dumont, F. M. Veronese, Selective alkylation and acylation of alpha and epsilon amino groups with PEG in a somatostatin analogue: tailored chemistry for optimized bioconjugates, Bioconjug. Chem. 13 (2002) 1238–1243.
[48] L. Yao, Z. Zhang, Q. Zhang, Z. Zhou, H. Yang, L. Chen, Modified organic polystyrene microspheres embedded into P(VDF-TrFE) with lotus-leaf microstructure enables high performance triboelectric nanogenerator, Nano Energy 86 (2021), 106128.
[49] L.L. Tan, W.J. Ong, S.P. Chai, A.R. Mohamed, Reduced graphene oxide-TiO_2 nanocomposite as a promising visible-light-active photocatalyst for the conversion of carbon dioxide, Nanoscale Res. Lett. 8 (2013) 465.
[50] V. Vinogradoff, F. Duvernay, G. Danger, P. Theulé, T. Chiavassa, C. Stehlé, C. Joblin, L. d'Hendecourt, Thermal evolution of interstellar ice analogues containing formaldehyde, EAS Publications Series 58 (2012) 337–341.
[51] Abdelfetteh Sayah, Farid Habelhames, Ahmed Bahloul, Belkacem Nessark, Yvan Bonnassieux, Denis Tendelier, Mohamed El Jouad, Electrochemical synthesis of polyaniline-exfoliated graphene compositefilms and their capacitance properties, J. Electroanal. Chem. 818 (2018) 26–34.
[52] N.A. Shepelin, N.A. Shepelin, V.C. Lussini, P.J. Fox, G.W. Dicinoski, A. M. Glushenkov, J.G. Shapter, A.V. Ellis, 3D printing of poly(vinylidene fluoride-trifluoroethylene): a poling-free technique to manufacture flexible and transparent piezoelectric generators, MRS Commun. 9 (2019) 159–164.
[53] Yanan Zhang, Yifei Zhao, Shaobo Tan, Zhicheng Zhang, Inserting –CH=CH– into P (VDF-TrFE) by C-F activation mediated with Cu(0) in a controlled atom transfer radical elimination process, Polym. Chem. 8 (11) (2017) 1840–1849.
[54] Krittish Roy, Sujoy Kumar Ghosh, Ayesha Sultana, Samiran Garain, Mengying Xie, Christopher Rhys Bowen, Karsten Henkel, Dieter Schmeiβer, Dipankar Mandal, A self-powered wearable pressure sensor and pyroelectric breathing sensor based on GO interfaced PVDF nanofibers, ACS Appl. Nano Mater. 2 (4) (2019) 2013–2025.
[55] Tingting Feng, Dan Xie, Yongyuan Zang, Xiao Wu, Tianling Ren, Wei Pan, Temperature control of P(VDF-TrFE) copolymer thin films, Integr. Ferroelectr. 141 (1) (2013) 187–194.
[56] D. Mao, B.E. Gnade, M.A. Quevedo-Lopez, Ferroelectric properties and polarization switching kinetic of poly (vinylidene fluoride-trifluoroethylene) copolymer, Ferroelectrics - Physical effects (2011) 77–100. Chapter 4.
[57] M. Stewart, M.G. Cain, D.A. Hall, Ferroelectric hysteresis measurement and analysis, NPL Report CMMT(A) (1999) 152.
[58] K.G. Ong, K. Zeng, C.A. Grimes, A wireless, passive carbon nanotube-based gas sensor, IEEE Sens. J. 2 (2002) 82–88.
[59] Dan Xu, Wenjie Zhao, Wenping Cao, Weili Li, Weidong Fei, Electrical properties of Li and Nb modified $BiFeO_3$ ceramics with reduced leakage current, Ceram. Int. 47 (3) (2021) 4217–4225.
[60] Y. Zhen, J. Arredondo, G.L. Zhao, Unusual dielectric loss properties of carbon nanotube—polyvinylidene fluoride composites in low frequency region (100 Hz < f < 1 MHz), Open J. Org. Polym. Mater. 3 (2013) 99–103.